Optimal conditions for thermal fixing of volume holograms in Fe:$LiNbO_3$ crystals

Chao Ray Hsieh, Shiuan Huei Lin, Ken Y. Hsu, Tai Chiung Hsieh, Arthur Chiou, and John Hong

We analyze and compare two typical recording and thermal fixing procedures of a volume hologram in a Fe:$LiNbO_3$ crystal (low–high–low procedure and high–low procedure). We consider the kinetics of the recording, compensating, and developing processes by taking into account the ratio of the conductivities between the protons and the electrons as a function of temperature. From the analysis the optimal environmental conditions (in terms of the fixing temperature and the compensation time) for each fixing procedure can be deduced for a crystal with given material parameters. © 1999 Optical Society of America

OCIS codes: 190.5330, 160.3730, 160.5320, 090.7330, 090.0090, 210.2860.

1. Introduction

Fixing of the refractive-index grating is one of the key issues for volume holographic memory. Thermal processing is by far the most popular and effective technique for storing nonvolatile photorefractive memories in Fe:$LiNbO_3$ crystals.[1–7] In general, thermal fixing is a means of transforming a photoinduced volatile (i.e., erasable by the readout beam) electronic grating into a nonvolatile ionic grating (which is insensitive to optical illumination) by means of the following three phases: (1) the recording phase, (2) the fixing (or the compensating) phase, and (3) the developing phase.[8–14] In the recording phase an electronic grating evolves in the crystal (by means of the photorefractive effect) in response to a nonuniform illumination of light. In the fixing (or the compensating) phase the crystal is heated to an elevated temperature (usually >400 K) when the protons (or the ions) migrate to form a complementary ionic grating. With opposite charge distributions the electronic and the ionic gratings compensate each other either partially or completely. In the developing phase the crystal (with the compensated grating pair) is cooled to near room temperature and then illuminated with a uniform (and preferably incoherent) developing beam. If the proton migration is negligible at near room temperature, the ionic grating will be frozen and developed (or manifested) when the electronic grating is gradually erased by the uniform developing beam. The main idea for those processes is that proton migration occurs at high temperature for the neutralization of the electronic grating, which is built at either low or high temperature. This ionic grating is not affected by light illumination at low temperature, and as a result the phase grating is fixed in the crystal. Thus thermally induced conductivities of the protons and the electrons at elevated temperature play the critical roles that determine the diffraction efficiency of the fixed grating. In terms of this viewpoint several models have been proposed to explain the mechanisms of the thermal fixing.[15–21] Above all, the efficiency and the lifetime of the fixing ionic grating are the main issues addressed in these proposals. In this paper we present our studies on the analysis of the thermal fixing by means of the kinetics of the recording, fixing, and developing processes for photorefractive memories in Fe:$LiNbO_3$ crystals. From the analysis we deduce the optimal environmental conditions for a crystal with a given iron-doped concentration. In particular, the influences

C. R. Hsieh, S. H. Lin, and K. Y. Hsu (ken@cc.nctu.edu.tw) are with the Institute of Electro-optical Engineering, National Chiao Tung University, Hsin-Chu, Taiwan. T. C. Hsieh is with the Department of Electro-Physics, National Chiao Tung University, Hsin-Chu, Taiwan. A. Chiou is with the Institute of Electrical Engineering, National Dong Hwa University, Hwa-Lien, Taiwan. J. Hong is with the Rockwell Science Center, 1049 Camino dos Rios, Thousand Oaks, California 91360.

Received 10 February 1999; revised manuscript received 27 May 1999.

0003-6935/99/296141-11$15.00/0

of the compensation time and the fixing temperature for given material parameters are presented.

2. Theoretical Analysis

Thermal fixing has been studied by many authors.[17,18] It was proposed that an ionic grating could be recorded in a photorefractive crystal through migration of protons inside the crystal as the crystal is elevated to a certain temperature. There are three processes involved: photoelectron grating buildup, proton migration and compensation, and ionic grating development. By taking into account the compensation effect of ions with the electronic grating in Kukhtarev's band transport model and following procedures similar to those in Kukhtarev's paper[22] (separating all parameters into dc terms and modulation terms and then solving the coupled material equations for the dc terms and the modulation terms, respectively; here we use subscript 0 as the dc term and subscript 1 as the modulation terms), we can obtain the dynamics of modulation of two space-charge densities, the empty electron trap density $[N_{D1}{}^{t}(t)]$, and the ion density $[n_{i1}(t)]$,

$$\frac{\partial N_{D1}{}^{t}(t)}{\partial t} = aN_{D1}{}^{t}(t) + bn_{i1}(t) + c, \tag{1}$$

$$\frac{\partial n_{i1}(t)}{\partial t} = dN_{D1}{}^{t}(t) + en_{i1}(t), \tag{2}$$

where

Table 1. Parameters Chosen for Numerical Calculation

Symbol	Parameter	Value[a]
s	Photoionization cross section	$0.2627\ \mathrm{cm^2\ J^{-1}}$
k_B	Boltzmann constant	$1.3805 \times 10^{-23}\ \mathrm{Jk^{-1}}$
γ_R	Recombination rate	$2.5 \times 10^{-8}\ \mathrm{cm^3\ s^{-1}}$
D_{i0}	Diffusion constant of ion	$0.081\ \mathrm{cm^2\ s^{-1}}$
ϵ_i	Activation energy of ion	1.1 eV
D_{e0}	Diffusion constant of electron	$65\ \mathrm{cm^2\ s^{-1}}$
ϵ_e	Activation energy of electron	0.2 eV
β_{i0}	Thermal ionization constant	$4 \times 10^{-3}\ \mathrm{s^{-1}}$
ϵ_D	Activation energy of thermal ionization	1 eV
N_D	Electronic doping density	$1.89 \times 10^{17}\ \mathrm{cm^{-3}}$
N_A	Electronic acceptor density	$6.3 \times 10^{16}\ \mathrm{cm^{-3}}$
n_{i0}	Ionic density	$10^{17}\ \mathrm{cm^{-3}}$
λ	Wavelength	514 nm
ϵ	Dielectric constant	$2.83 \times 10^{-10}\ \mathrm{fm^{-1}}$
P	Photovoltaic constant	$3.81 \times 10^{-26}\ \mathrm{cm^3\ V^{-1}}$
θ	Bragg angle	20°
I_0	dc term of light intensity	$150\ \mathrm{mW\ cm^{-2}}$
I_1	Modulation term of light intensity	$50\ \mathrm{mW\ cm^{-2}}$
n_{e0}	dc term of electron density	
D_e	Diffusion coefficient of electron	
D_i	Diffusion coefficient of ion	
β	Thermal ionization coefficient	
μ_e	Electronic mobility	
μ_i	Ionic mobility	
Q_e	Electron surface charge density	
Q_i	Ion surface charge density	
K	Grating spacing	
A–D	Integral constant	

[a]Ref. 18.

$$a = -\frac{\omega_e\gamma_R N_A + (sI_0 + \beta)\frac{N_D}{N_A}(\omega_e + D_eK^2 + j\mu_eKE_0) + j\frac{PI_0K}{q}\gamma_R N_A}{\gamma_R N_A + \omega_e + D_eK^2 + j\mu_eKE_0}, \tag{3}$$

$$b = -\frac{\omega_e\gamma_R N_A}{\gamma_R N_A + \omega_e + D_eK^2 + j\mu_eKE_0}, \tag{4}$$

$$c = \frac{jK\frac{P(N_D - N_A)}{q}I_1 - s(N_D - N_A)I_1}{\gamma_R N_A + \omega_e + D_eK^2 + j\mu_eKE_0}\gamma_R N_A + s(N_D - N_A)I_1, \tag{5}$$

$$d = -\omega_i, \tag{6}$$

$$e = -(\omega_i + D_iK^2 - j\mu_iKE_0), \tag{7}$$

where

$$\omega_e \equiv q\mu_e n_{e0}/\epsilon, \text{ the electronic dielectric relaxation rate,} \tag{8}$$

$$\omega_i \equiv q\mu_i n_{i0}/\epsilon, \text{ the ionic dielectric relaxation rate.} \tag{9}$$

The definitions and the values of all parameters are listed in Table 1. By substituting the space-charge distribution into Poisson's equation, we can write the space-charge field in the crystal as

$$E_{sc}(t) = E_0 + E_1(t)[\exp(-jKx) + \text{c.c.}], \tag{10}$$

where

$$E_1(t) = \frac{jq}{\epsilon K}[N_{D1}{}^{t}(t) + n_{i1}(t)]. \tag{11}$$

Note that, in Eq. (10), E_0 represents the dc term of the space-charge field. To calculate $E_{sc}(t)$, Eqs. (1)

and (2) should be solved with appropriate boundary conditions. In practice there are two cases: with and without an externally applied field. In the first case E_0 remains constant during the grating recording period (representing short-circuit or preexposed open-circuit boundary conditions). Equations (1) and (2) can be turned into a set of linear differential equations with constant coefficients. Under this situation an analytic solution for thermal fixing can be obtained. However, in the second case (representing open-circuit boundary condition), because of the photovoltaic effect, photoexcited carriers will be gradually cumulated on the boundaries of the crystal to develop an open-circuit voltage under light illumination. The dc term of the space-charge field, E_0, then becomes a temporal function whose time scale is close to the photorefractive time constant. Under this situation Eq. (1) and (2) become nonlinear differential equations. We need to solve the temporal growth of the dc term $E_0(t)$ first; then the space-charge field [Eqs. (1) and (2)] can be solved by numerical methods. In summary, Eqs. (1)–(11) represent a general description of the temporal behavior of the thermal fixing grating. The solution of those equations depends on the boundary conditions of the crystal as well as on the initial conditions of ${N_{D1}}^t$ and n_{i1} for each thermal fixing procedure.

For each of the two kinds of boundary conditions two thermal fixing procedures have been practiced[17,18]: (i) the low–high–low (L–H–L) procedure and (ii) the high–low (H–L) procedure or the simultaneous recording and compensating procedure. In the L–H–L procedure an electronic grating is first recorded by illumination of the crystal with the recording beams at low temperature (usually at room temperature, at which proton migration is negligible). The protons are then thermally activated to form an ionic grating that neutralizes the electronic grating when the crystal is heated to high temperature without light illumination. Finally the ionic grating is developed by a non-Bragg-matched uniform beam at low temperature. In the H–L procedure the recording and the compensating processes occur simultaneously by illumination of the crystal with the recording beams at high temperature, and the developing process is then carried out at low temperature. Each phase of the above procedures produces different initial conditions for the differential equations [Eqs. (1) and (2)].

To provide a better vision of the kinetics of the fixing procedures, we perform a computer evaluation for both fixing procedures under different boundary conditions. Before doing that, we show a qualitative analysis of the thermal fixing within the framework of the conductivity properties of the electrons and the protons. Because the thermal fixing process depends crucially on the migration of the protons at high temperature, the ratio of the ionic conductivity and the electronic conductivity as a function of temperature plays a key role in thermal fixing. The

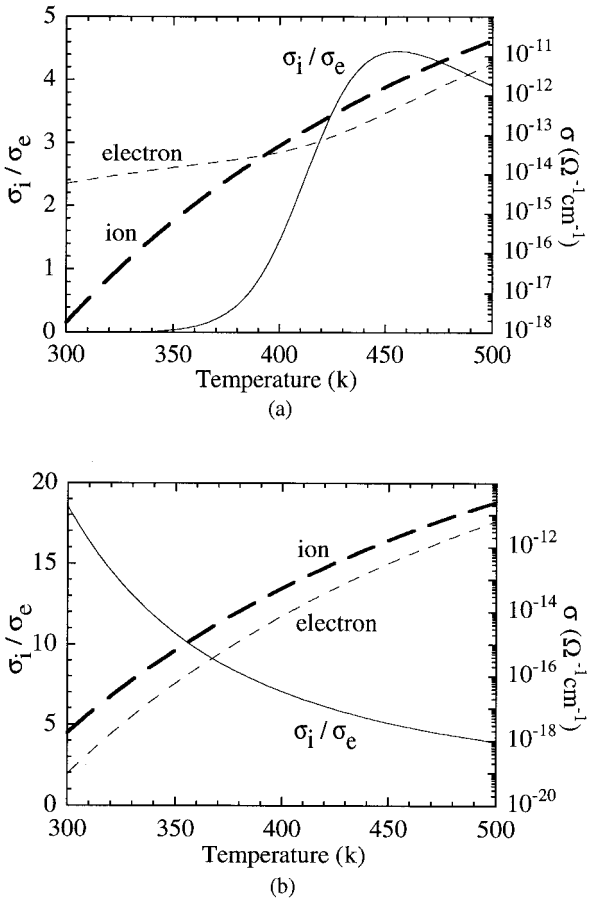

Fig. 1. Ratio of the ionic conductivity and the electronic conductivity and the absolute value of the ionic conductivity as a function of temperature: (a) under light illumination of intensity 150 mW cm^{-2}, (b) in dark.

thermally dependent conductivities of the electrons and the protons are considered and expressed as

$$\sigma_e(T) = q\mu_e n_{e0} = \frac{q^2(N_D - N_A)}{k_B T \gamma_R N_A}\,[sI_0 + \beta_0 \exp(-\epsilon_D/k_B T)] \times [D_{e0} \exp(-\epsilon_e/k_B T)], \tag{12}$$

$$\sigma_i(T) = q\mu_i n_{i0} = \frac{q^2 n_{i0}}{k_B T}\,[D_{i0} \exp(-\epsilon_i/k_B T)]. \tag{13}$$

The ratio of the ionic to the electronic conductivities is shown in Fig. 1(a) for the case in which the crystal is under light illumination of intensity 150 mW cm^{-2}. This corresponds to both the recording and the developing phases in the L–H–L procedure and to the simultaneous recording and compensation and the developing phases in the H–L procedure. This ratio is shown in Fig. 1(b) for the case in which the crystal is kept in the dark, which corresponds to the compensating phase in the L–H–L procedure. It can be seen from Fig. 1(a) that the ionic conductivity is negligibly small at room temperature; the ratio becomes larger than 1 when the temperature is raised to above 390 K, and it reaches a maximum value at ~450 K. This explains qualitatively why net electronic grating

could be built up during the recording phase in the L–H–L procedure, why the crystal should be heated to an elevated temperature during the simultaneous recording and compensating phase in the H–L procedure, and why the ionic grating can be revealed by light illuminated at low temperature for both the L–H–L and the H–L procedures. However, Fig. 1(b) shows that the ratio is always larger than 1 in the dark for the present range of temperature. This means that the conductivity that is due to thermal excitation for ions is always larger than that of the electrons. This implies that, in the L–H–L procedure, the ionic grating compensating process could be carried out at any temperature. However, at room temperature the absolute values of the ionic and the electronic conductivities are negligibly small such that the time needed to reach complete compensation becomes unacceptably long (the time constant is approximately 9×10^7 s at room temperature, which is shown in Section 3). Thermal fixing of the grating at low temperature is not practical. Therefore, to build up an efficient ionic grating within acceptable finite time, it is necessary to heat the crystal to appropriate temperatures. At elevated temperatures, the ionic conductivity is dominant and the ions readily compensate for the electronic grating. Finally, it is worth noting from Fig. 1 that at low temperatures the ionic conductivity is always so small as to be negligible, and thus the ionic grating maintains at the state of quasi-permanent storage.

3. Analysis of Thermal Fixing Dynamics

In this section we use computer evaluation to study the dynamics of thermal fixing for the above two procedures under short-circuit and open-circuit cases, respectively, and then determine the optimal conditions of the thermal fixing, in terms of compensation time and temperature.

A. Short-Circuit Case

An analytic solution for the space-charge field can be solved for each phase and is given as

$$E_1(t) = \frac{jq}{\epsilon K}\left[(A + B)\exp(-t/\tau_1) + (C + D)\exp(-t/\tau_2) + \frac{c(d - e)}{ae - bd}\right], \tag{14}$$

where

$$\tau_1 = -\frac{2}{(a + e) + [(a + e)^2 - 4(ae - bd)]^{1/2}}, \tag{15}$$

$$\tau_2 = -\frac{2}{(a + e) - [(a + e)^2 - 4(ae - bd)]^{1/2}}, \tag{16}$$

where A–D are four integral constants that can be determined by the initial conditions of $N_{D1}{}^t$ and n_{i1} in each process, respectively. In Eq. (14) it is seen that there are two time constants related to the temporal response of the space-charge field. This implies that there are two different factors that simultaneously affect the kinetics of the thermal fixing. It is plausible to consider that one is for the ionic grating and the other is for the electronic grating. Below we see that τ_2 is related to the electronic grating growth and τ_1 is related to the ionic grating growth.

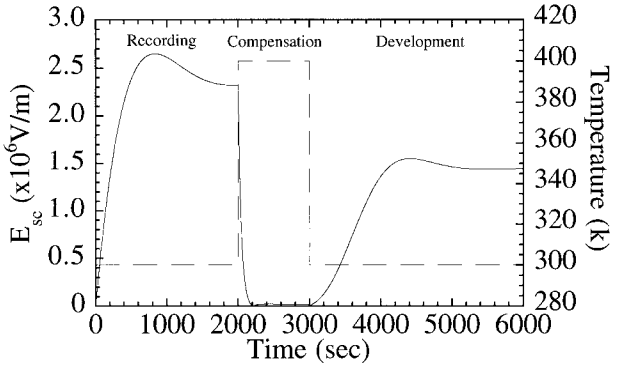

Fig. 2. Typical temporal behaviors of the strength of E_{sc} and the temperature for a L–H–L procedure.

1. Low–High–Low Process

By using Eq. (14) we obtain a temporal variation of the strength of the space-charge field, E_{sc}, with the corresponding crystal temperature for a L–H–L procedure, as shown in Fig. 2. In the recording phase ($0 < t < t_r$) the crystal is kept at near room temperature while illuminated by the reference and the object waves. Since, in the beginning, the grating was not yet recorded in the crystal, the initial conditions are $N_{D1}{}^t(0) = 0$ and $n_{i1}(0) = 0$. The modulation of the space charge $N_{D1}{}^t(t)$ and $n_{i1}(t)$ can be written as

$$N_{D1}{}^t(t) = \left[-\tau_1 c + \frac{\tau_1}{\tau_1 - \tau_2}\left(\frac{ce}{ae - bd} + \tau_1 c\right)\right]\exp(-t/\tau_1) - \left[\frac{\tau_2}{\tau_1 - \tau_2}\left(\frac{ce}{ae - bd} + \tau_1 c\right)\right]\exp(-t/\tau_2) - \frac{ce}{ae - bd}, \tag{17a}$$

$$n_{i1}(t) = \frac{cd}{ae - bd}\left[1 - \frac{\tau_1}{\tau_1 - \tau_2}\exp(-t/\tau_1) + \frac{\tau_2}{\tau_1 - \tau_2}\exp(-t/\tau_2)\right]. \tag{17b}$$

Figures 3(a) and 3(b) show the dynamics of $N_{D1}{}^t(t)$ and $n_{i1}(t)$, respectively, for the case of $I_0 = 150$ mW cm^{-2}, $I_1 = 50$ mW cm^{-2}, and $T = 300$ K. It is seen that $N_{D1}{}^t(t)$ tends to increase rapidly and that $n_{i1}(t)$ rarely compensates the electronic field, because the values of $n_{i1}(t)$ are 3 orders of magnitude less than that of $N_{D1}{}^t(t)$. This means that, at low temperature, although the protons are movable to form an ionic grating, the conductivity of protons is much smaller than that of electrons under light illumination; consequently, the proton compensation is too slow to neu-

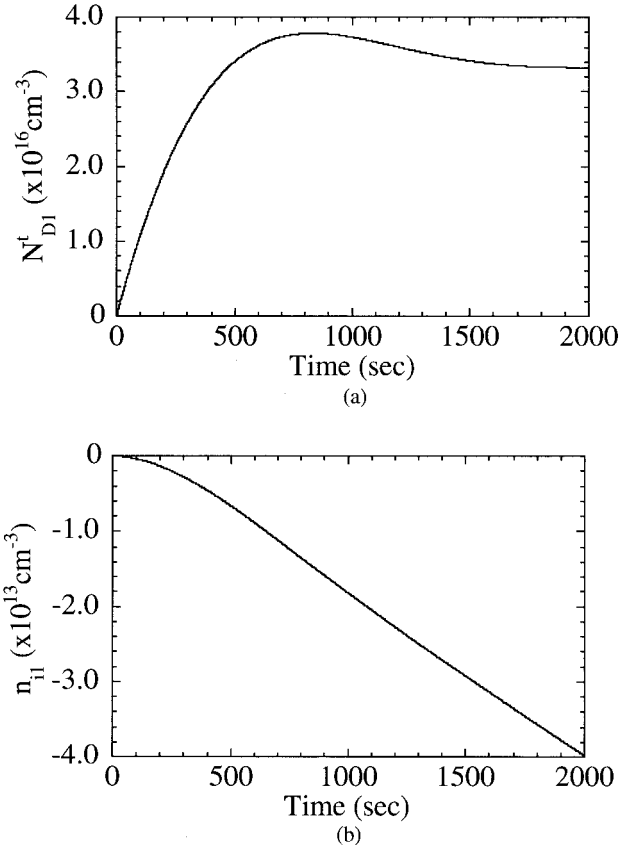

Fig. 3. Dynamics of (a) $N_{D1}{}^t(t)$ and (b) $n_{i1}(t)$ for the case of $I_0 = 150$ mW cm^{-2}, $I_1 = 50$ mW cm^{-2}, and $T = 300$ K in the recording phase for a L–H–L procedure.

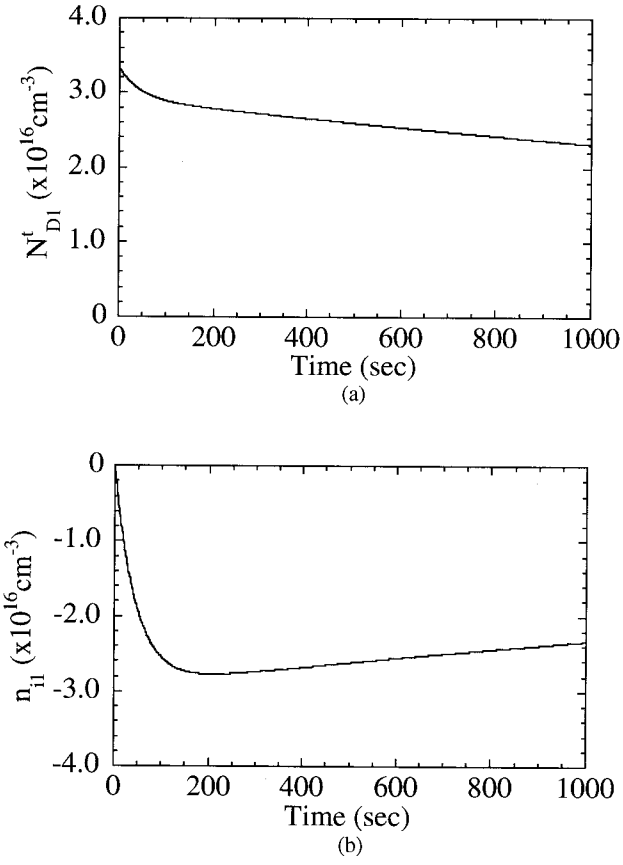

Fig. 4. Dynamics of (a) $N_{D1}{}^t(t)$ and (b) $n_{i1}(t)$ for the compensating phase for a L–H–H procedure and $T = 400$ K.

tralize the electronic grating in finite time. The net space-charge field therefore increases as the electronic grating builds up (as shown in phase I in Fig. 2).

When the electron grating reaches saturation at $t = t_r$ (we take 2000 s for recording), both recording beams are cut off and the crystal is heated to a high temperature. Before the beginning of the compensating phase ($t_r \le t < t_r + t_c$), an electronic grating was recorded during the recording phase and is rarely compensated by protons. Therefore the initial conditions for the compensation phase are taken as $N_{D1}{}^t(t = t_r) = N_{D1}{}^t(t_r)$ and $n_{i1}(t = t_r) = 0$. The modulation of the space charge $N_{D1}{}^t(t)$ and $n_{i1}(t)$ can be written as

$$N_{D1}{}^t(t) = \frac{\tau_1\tau_2}{\tau_1 - \tau_2} N_{D1}{}^t(t_r) \times \left\{ \begin{matrix} -\left(\frac{1}{\tau_2} + a\right)\exp[-(t - t_r)/\tau_1] \\ +\left(\frac{1}{\tau_1} + a\right)\exp[-(t - t_r)/\tau_2] \end{matrix} \right\}, \qquad t \ge t_r, \tag{18a}$$

$$n_{i1}(t) = \frac{\tau_1\tau_2}{\tau_1 - \tau_2} dN_{D1}{}^t(t_r)\{\exp[-(t - t_r)/\tau_1] - \exp[-(t - t_r)/\tau_2]\}, \qquad t \ge t_r. \tag{18b}$$

Note that in Eqs. (18) two exponential terms with different signs and different time constants τ_1 and τ_2 are involved in the development of the thermally fixed ionic grating. It is interesting to see the physical mechanisms that are related to τ_1 and τ_2. During the compensation phase no light is illuminated on the crystal. Thus $I_0 = I_1 = 0$, which results in $b = c = 0$ in Eqs. (4) and (5). Furthermore, from Fig. 1(b), the thermal-excitation conductivity of electrons is always smaller than that of ions. If for the moment one neglects thermal excitation of the electrons, then $a = 0$ in Eq. (3). Thus, for Eq. (1), $N_{D1}{}^t(t)$ stays constant in time. Under this situation one finds by Eq. (16) that τ_2 is infinite. Therefore, from Eq. (18a), $N_{D1}{}^t(t)$ becomes $N_{D1}{}^t(t_r)$, which is the initial value of this phase. From Eq. (18b) the time-dependent function of the proton grating growth, $n_{i1}(t)$, now becomes $\tau_1 dN_{D1}{}^t(t_r)\exp[-(t - t_r)/\tau_1]$. This implies that in Eq. (18b) the former term contributes to the growth of the ionic grating and that the latter term reduces the growth of the ionic grating, which results from thermal erasure of the electron grating. In other words, τ_1 is related to the buildup of the ionic grating, and τ_2 is related to that of the electronic grating.

Figures 4(a) and 4(b) show the dynamics of $N_{D1}{}^t(t)$ and $n_{i1}(t)$, respectively, for the case in which temperature $T = 400$ K. It is seen that in Fig. 4(a) the

modulation $N_{D1}{}^{t}(t)$ first drops a little, quickly, and then decreases, slowly. In Fig. 4(b) the modulation $n_{i1}(t)$ shows a similar trend. Note that at high temperature both electrons and protons have high mobilities. In the beginning of the compensating phase the drift effect produced by the space-charge field of the initial electronic grating makes thermally excited electrons and protons move to neutralize each other. This process is faster than that of the electronic grating erasure, which is caused by the diffusion effect of the thermally excited electrons. Thus the compensation takes place at a high rate until the electronic grating has been compensated completely. In other words, the grating compensation is actually complete in the short beginning period. Further compensation will cause a decay of both the electronic and the ionic gratings as a result of the thermally excited effect.

The growth of the ionic grating depends crucially on the temperature, T. Typically, the higher the temperature, the larger the compensation rate and thus the faster the ionic grating growth rate. However, higher temperatures also cause a faster decay of the electronic grating (by means of thermal excitation), and it tends to reduce the strength of the compensating ionic grating. Therefore there is a trade-off between the compensation time and the fixing temperature to obtain the optimal conditions for maximizing the diffraction efficiency of the fixed grating. The guidelines for choosing the optimal conditions are presented later in this section.

In the developing phase ($t_r + t_c + t_d \geq t \geq t_r + t_c \approx$ 3000 s in Fig. 2), the crystal is cooled to room temperature and then illuminated by a non-Bragg-matched beam. The light beam causes partial redistribution of the trapped electrons by photoexcitation and thereby reveals the ionic grating, which manifests itself as the space-charge field is built up. Since the electronic and the ionic gratings have been building up in the compensating state and since the compensation time is t_c, the initial conditions for the development phase are taken as $N_{D1}{}^{t}(t_r + t_c)$ and $n_{i1}(t_r + t_c)$. The modulations of the space charge, $N_{D1}{}^{t}(t)$ and $n_{i1}(t)$, can be written as

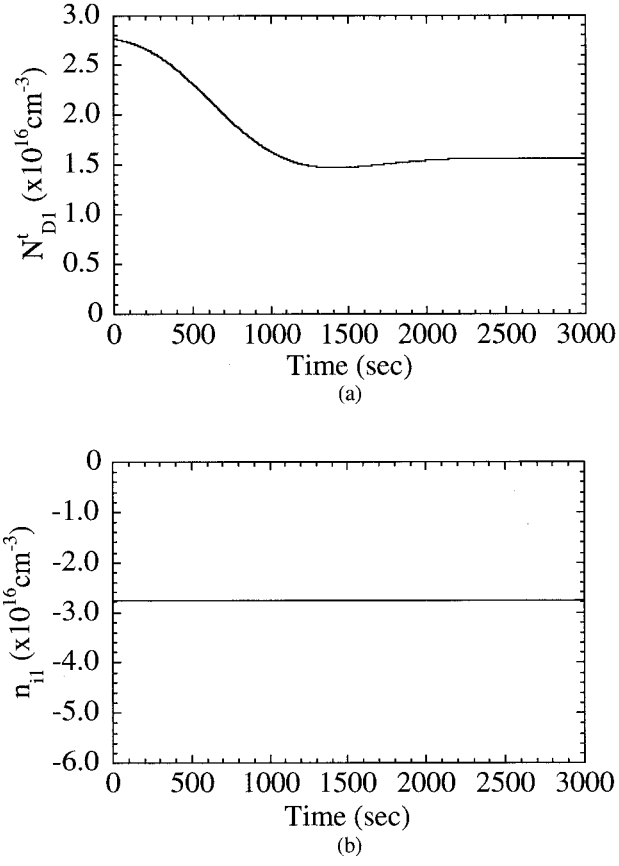

Fig. 5. Dynamics of (a) $N_{D1}{}^{t}(t)$ and (b) $n_{i1}(t)$ for the developing phase for a L–H–H procedure; $I_0 = 150$ mW cm^{-2}, and $T = 300$ K.

$$N_{D1}{}^{t}(t) = \frac{\tau_1\tau_2}{\tau_1 - \tau_2}\left(\begin{array}{l} -\left[\left(\frac{1}{\tau_2} + a\right)N_{D1}{}^{t}(t_r + t_c) + bn_{i1}(t_4 + t_c)\right]\exp\{-[t - (t_r + t_c)]/\tau_1\} \\ +\left[\left(\frac{1}{\tau_1} + a\right)N_{D1}{}^{t}(t_r + t_c) + bn_{i1}(t_r + t_c)\right]\exp\{-[t - (t_r + t_c)]/\tau_2\} \end{array}\right), \qquad t \geq t_r + t_c, \tag{19a}$$

$$n_{i1}(t) = \frac{\tau_1\tau_2}{\tau_1 - \tau_2}\left(\begin{array}{l} -\left[\left(\frac{1}{\tau_2} + f\right)n_{i1}(t_r + t_c) + dN_{D1}{}^{t}(t_r + t_c)\right]\exp\{-[t - (t_r + t_c)]/\tau_1\} \\ +\left[\left(\frac{1}{\tau_1} + f\right)n_{i1}(t_r + t_c) + dN_{D1}{}^{t}(t_r + t_c)\right]\exp\{-[t - (t_r + t_c)]/\tau 2\} \end{array}\right), \qquad t \geq t_r + t_c. \tag{19b}$$

Figures 5(a) and 5(b) show the dynamics of $N_{D1}{}^{t}(t)$ and $n_{i1}(t)$, respectively, for the case $I_0 = 150$ mW cm^{-2} and $T = 300$ K. It is seen that in Fig. 5(b) the $n_{i1}(t)$ modulation keeps essentially constant through-

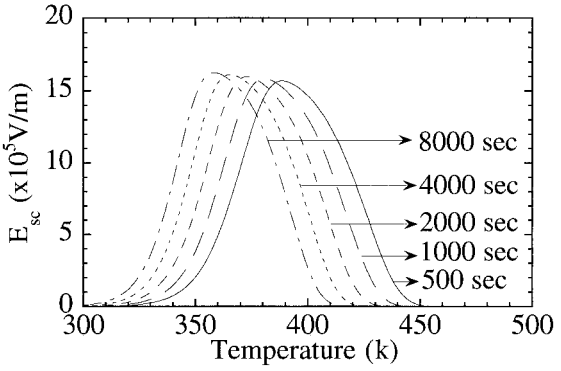

Fig. 6. Final strength of the space-charge field as a function of temperature for compensation time t_c in the range of 500–8000 s for a L–H–L procedure.

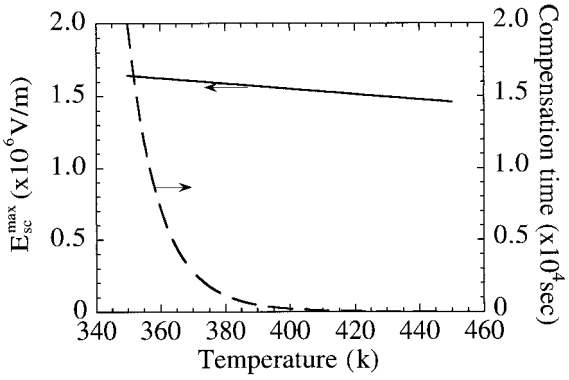

Fig. 7. Maximum reachable strength of the space-charge field and the required compensation time as a function of temperature for a L–H–L procedure under the short-circuit condition.

out this phase because of the low ionic conductivity at this temperature. However, in Fig. 5(a), the $N_{D1}{}^{t}(t)$ modulation first decreases rapidly when the electronic grating is erased by photoexcitation. It then decreases slowly by the residual intrinsic ionic migration at low temperature. As a result the space-charge field increases up to a saturated value that is determined by the degree of redistribution of previously trapped electrons. The required developing time can be defined as the time required for the modulation $N_{D1}{}^{t}(t)$ to reach the local minimum values. Therefore the developing time can be determined by use of Eq. (19a). For the example shown in Fig. 5(a) it is ~1350 s. It is interesting to note that during the readout stage the fixed grating is illuminated by a weak probe beam. The lifetime of the grating is determined by the decay time of the ionic grating. By using Eq. (19b) with parameters in Table 1, we can estimate the lifetime of an ionic grating in $LiNbO_3$:Fe at room temperature to be ~3 yr.

Now the final strength of the space-charge field can be obtained. Note that, during the recording and the developing phases in the L–H–L procedure, which occur at low temperature, only photoinduced electronic gratings are involved in the dynamics. The compensation temperature and time at high temperature play a crucial role for determining the grating strength of the ionic grating. In other words, the final strength of the space-charge field (immediately after the developing procedure) is determined by the compensation temperature and time. Figure 6 shows the final strength of the space-charge field as a function of compensation temperature for various compensation times t_c in the range of 500–8000 s. Note that for a given t_c the strength of the space-charge field increases with temperature, reaches a maximum value near T = 350–390 K, and then decreases with temperature, owing to thermal excitation of the charge carriers. The higher the temperature, the greater the reduction of the peak space-charge field. It is also seen that both the location and the magnitude of the peak space-charge field depend on the compensation time. Larger peaks occur at lower temperature, provided that we take longer compensation time. Although the magnitude of the peak increases as the compensation time increases, the effect is relatively mild for the long compensation time in the range of 1000–8000 s.

By differentiating Eq. (18b) with respect to time, we can obtain a required compensation time t_c for reaching the maximum magnitude of the ionic grating $n_{i1}(t)$. Both the maximum magnitude and the required compensation time are functions of the compensation temperature. Therefore the maximum of the space-charge field that can be revealed after developing can be obtained. The results of the numerical calculation are shown in Fig. 7. It is seen that the magnitude of the maximum space-charge field and the required compensation time both decrease with temperature. The figure provides us a useful guide for designing the fixing environments. By using this plot, for a given temperature, we can determine the required compensation time t_c for maximizing the space-charge field. The figure also shows that, in principle, the ionic fixing can be carried out at virtually any temperature, provided that a sufficiently long compensation time is allowed. This is again in agreement with the description in Section 2. In the example considered here, t_c = 2000 s and T = 373 K represent an appropriate condition and the compensation efficiency [defined by $|n_{i1}(t_r + t_c)/N_{D1}{}^{t}(t_r)|$] is ~82%, which is suitable for the experimental implementations.

2. *High–Low Process*

In the H–L procedure the crystal is heated to an elevated temperature (usually >370 K) first and then illuminated by both the reference and the object beams for recording holograms. Since, at high temperature, the protons (or ions) easily migrate to form a complementary ionic grating, the recording of the photoelectronic grating and compensating of the ionic grating occur simultaneously. There is no need for a separate compensating phase. The compensation is automatically achieved during the recording procedure. Because no grating has been recorded before the beginning of the recording phase, the initial conditions are set as $N_{D1}{}^{t}(0) = 0$ and $n_{i1}(0) = 0$. Thus

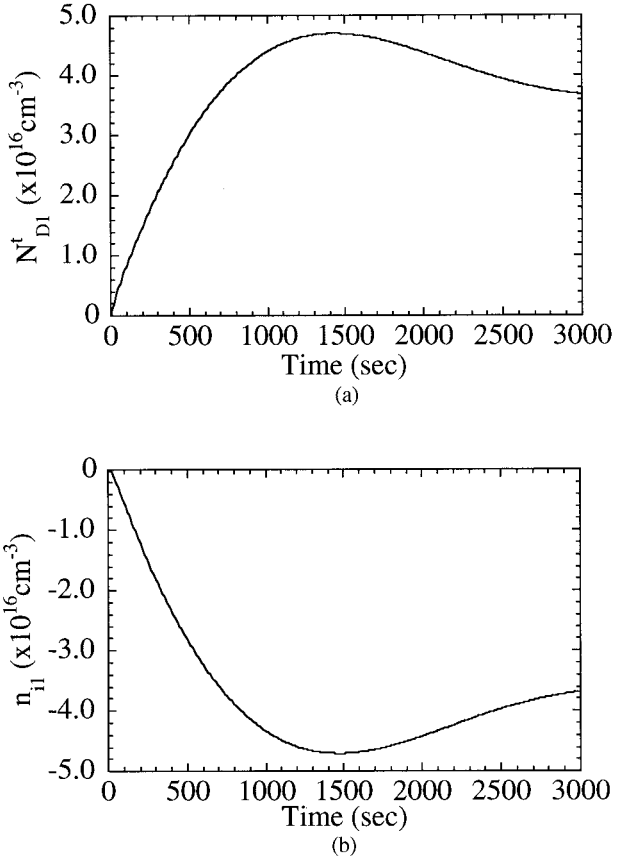

Fig. 8. Dynamics of (a) $N_{D1}{}^t(t)$ and (b) $n_{i1}(t)$ for the recording and the compensation phase for a H–L procedure; $I_0 = 150$ mW cm^{-2}, $I_1 = 50$ mW cm^{-2}, and $T = 400$ K.

the dynamics of the modulation of the space charge is governed by the same formulas as in Eqs. (17a) and (17b), except with all parameters taken at high temperature. As an example, Figs. 8(a) and 8(b) show the dynamics of $N_{D1}{}^t(t)$ and $n_{i1}(t)$, respectively, for the case of $I_0 = 150$ mW cm^{-2}, $I_1 = 50$ mW cm^{-2}, and $T = 400$ K. First, it is seen that the magnitude of the modulation $n_{i1}(t)$ is the same order as that of the modulations $N_{D1}{}^t(t)$. This indicates that, at high temperature, the protons are allowed to move to form a complementary ionic grating at the same speed as when electronic gratings are formed. It is also seen that both $N_{D1}{}^t(t)$ and $n_{i1}(t)$ oscillate as time increases. This effect occurs because, under optical illumination, the photovoltaic effect is large enough to provide an imaginary part of the response time, which makes the modulation terms oscillate. Similar to the L–H–L case, the fixed ionic grating strength depends crucially on the recording time and temperature. To obtain the maximum space-charge field, we should carefully choose the recording time such that the ionic grating strength is maximized. We can achieve this by ending the recording phase at the time when $N_{D1}{}^t(t)$ reaches the first peak. For the case in Fig. 8(a) the recording time could be selected to be ~1400 s.

In the developing phase both the reference and the object beams are cut off, the crystal is cooled down to room temperature, and then the ionic grating is developed while the crystal is illuminated by a non-Bragg-matched uniform beam. Because the environmental conditions in this phase are the same as those in the L–H–L procedure, the dynamics of $N_{D1}{}^t(t)$ and $n_{i1}(t)$ are the same as those in the L–H–L procedure, which are governed by Eqs. (19a) and (19b).

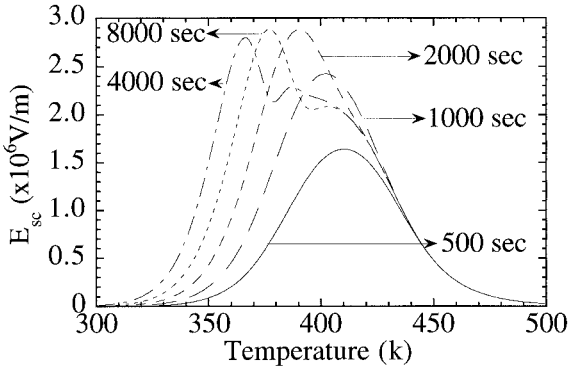

Fig. 9. Final strength of the space-charge field as a function of temperature for various compensation times t_c in the range of 500–8000 s for a H–L procedure.

Using Eqs. (17a) and (17b) and (19a) and (19b), we can obtain the complete dynamics of thermal fixing for H–L procedure. The dependence of the final strength of the space-charge field on the recording temperature is plotted in Fig. 9 for various recording times in the range of 500–8000 s. It is seen that for a short recording time (e.g., 500 s) the space-charge field increases as the recording temperature increases from room temperature, reaching a maximum value near $T = 390$–420 K. Further temperature increase causes the grating strength to decrease, because the uniform thermal excitation tends to dominate over the photoexcitation of the interference fringes [as shown in Fig. 1(a)]. However, for long recording time (e.g., $t_r > 4000$ s), the strength of the fixed space-charge field oscillates, owing to the large photovoltaic effect in the $LiNbO_3$ crystal.[23] To maximize the strength of the fixed grating, the fixing procedures (in terms of recording time and temperature) should be carefully designed. Figure 10 shows the reachable maximum strength of the space-charge field and the required recording time as a function of temperature. The two curves shown in Fig. 10 provide us with a useful guide for designing the fixing procedure in the H–L procedure. First, it is seen that there exists a temperature for which the reachable grating strength is at maximum. This is called the optimal temperature for the H–L process. In our case this occurs at ~380 K. Figure 10 also shows that the required recording time decreases monotonically as the temperature is raised above optimum. This is in agreement with the result shown in Fig. 1(a), where an optimal temperature exists for obtaining a unit conductivity ratio such that the compensating efficiency is maximized.

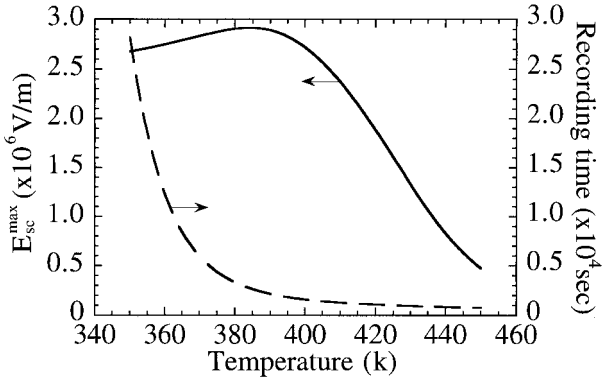

Fig. 10. Maximum reachable strength of the space-charge field and the required recording time as a function of temperature for a H–L procedure under the short-circuit condition.

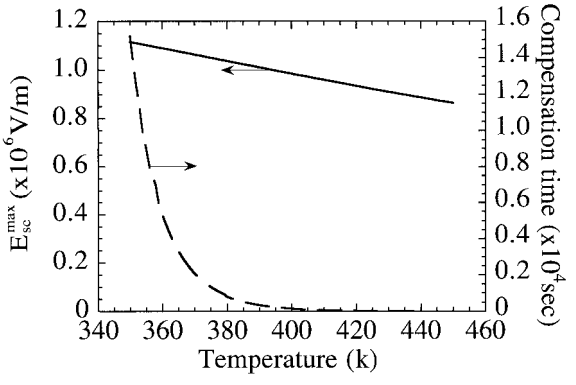

Fig. 11. Maximum reachable strength of the space-charge field and the required compensation time as a function of temperature for a L–H–L procedure under the open-circuit condition.

For temperatures below the optimal value the reachable maximum grating strength is seen to be reduced only slightly. However, recording at excessively low temperature is undesirable, since it takes an unacceptably long time to complete the proton–electron compensation. Therefore there is a trade-off between the recording time t_r and the temperature T.

B. Open-Circuit Case

Once the external constant dc field on the boundary of the crystal is removed, an open-circuit voltage will be developed across the two ends of the grating vector during each phase of recording, compensation, and developing. The temporal behavior of the dc field growth should be evaluated before we calculate the space-charge field.

$E_0(t)$ can be obtained by calculation of the surface-charge density $\sigma(t)$ at the end surface of the crystal under light illumination.[23] By substituting the surface-charge density into the current density formula ($J_{e0} = dQ_e/dt$ for electron, $J_{i0} = dQ_i/dt$ for proton) and the Poisson's equation ($E_0 = Q_i - Q_e/\epsilon$), the temporal behavior of the dc field can be solved for each phase. In the recording phase $E_0(t)$ grows during the recording and can be written as

$$E_0(t) = E_{0ph}\{1 - \exp[-(\omega_e + \omega_i)t]\}, \tag{20}$$

where

$$E_{0ph} = -\frac{PI_0(N_D - N_A)}{q(\mu_e n_{e0} + \mu_i n_{i0})}, \tag{21}$$

where E_{0ph} is the saturated photovoltaic field and ω_e, ω_i are the dielectric relaxation rates, which are given by Eqs. (8) and (9). Comparing dielectric relaxation time (i.e., $1/\omega_e$, $1/\omega_i$) with Eqs. (15) and (16), we found that the time constant for E_0 and that for the recording phase have the same order of magnitude. Therefore, the dc field cannot be assumed to be a constant during grating recording.

In the compensation phase the photovoltaic effect, which was the effect of driving the photoionized carriers to the end surface of the crystal, is removed, because all the recording beams are turned off. The photovoltaic field that was built up by the recording beams starts to decay, because of the high conductivity of the thermally excited electrons and protons. The electrons neutralize and the protons compensate the surface charges on the boundaries of the crystal such that the dc field drops from an initial value of $E_0(t_r)$ (where t_r is the recording time). The dc field can therefore be given as

$$E_0(t) = E_0(t_r)\exp[-(\omega_e + \omega_i)t], \tag{22}$$

where ω_e, ω_i have been defined as in Eqs. (8) and (9). However, because of the strong dependence of n_{e0} on the light intensity and on the thermal excitation of photocarriers, the value of ω_e, ω_i in the compensation phase is different from that in the recording phase.

In the development phase the photovoltaic effect is revealed again because of the illumination by a uniform developing beam. $E_0(t)$ grows from the initial field $E_0(t_c)$, which is the remaining field at the end of compensation, and can therefore be given as

$$E_0(t) = E_{0ph}\{1 - \exp[-(\omega_e + \omega_i)t]\} + E_0(t_c) \times \exp[-(\omega_e + \omega_i)t], \tag{23}$$

where E_{0ph}, ω_e, ω_i are given by Eq. (21) and Eqs. (8) and (9), respectively. By substituting Eqs. (20)–(23) and Eqs. (8) and (9) into Eqs. (1) and (2), we can evaluate the temporal dynamics of the thermal fixing for various temperature conditions by using the fifth-order Runge–Kutta numerical method.

Again, the reachable maximum space-charge field and the required compensation time with respect to the temperature for both the L–H–L and the H–L fixing procedures can be obtained. The results are plotted in Figs. 11 and 12, respectively. Those two figures are a useful guide for designing the environmental conditions of the thermal fixing under the open-circuit boundary condition. Comparing Fig. 11 with Fig. 7, we see that the maximum space-charge field and the required compensation time for both L–H–L procedures show the same trend. However, the absolute value of the space-charge field for the

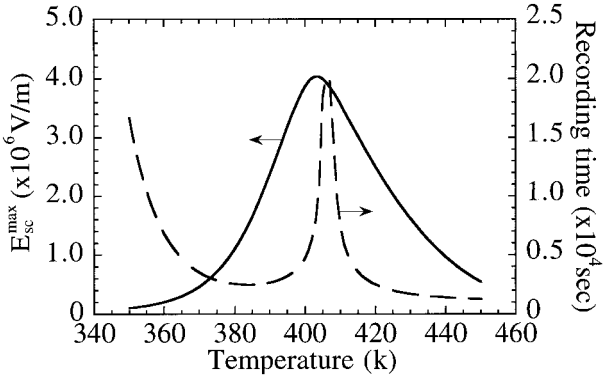

Fig. 12. Maximum reachable strength of the space-charge field and the required recording time as a function of temperature for a H–L procedure under the open-circuit condition.

open-circuit case is somewhat smaller than that for the short-circuit case (~25% less). However, comparing Fig. 12 with Fig. 10, we see that the maximum space-charge field for the H–L procedures under the open-circuit condition drops significantly in the low temperature range and that the absolute value for the open-circuit case in the low temperature range is the smallest among the four cases. We believe that this significant drop results from the low grating strength during the recording phase. Note that it is interesting to see the resulting curve of the required recording time as a function of the recording temperature. The recording time first decreases quickly as the temperature increases. The trend of the curve is similar to that in Fig. 10. However, when the temperature is close to the point of equal conductivity for the electrons and the protons such that the net effect of the dc field is weak, the oscillation phenomena that are due to the photovoltaic effect during recording will not occur. Under this condition the maximum value of the space-charge field can be increased, provided long recording time is allowed. Therefore the required recording time increases near this temperature. As the temperature is increased above this point, thermal excitation of electrons become stronger and thus the recording strength is again decreased.

4. Conclusion

By considering the thermal and the photoexcitation effects on the conductivities of protons and electrons, we have investigated the kinetic behavior of the thermal fixing of the photorefractive grating in a Fe: $LiNbO_3$ crystal. The thermal fixing properties in each phase have been analyzed in terms of the competition of the kinetics of the electronic and the ionic gratings modulation. Our theoretical analysis and computer simulation show that two operation parameters for optimizing grating fixing efficiency are the compensation temperature and time. We have developed a technique for selecting optimal operation conditions. In the L–H–L procedure the electronic gratings are recorded at low temperature, whereas the proton–electron compensation occurs at high temperature in the dark. In this case, the compensation efficiency is higher with lower compensation temperature and the compensation could be carried out at any temperature, provided a long compensation time is allowed. However, the compensation time required for reaching a complete compensation at low temperature is unacceptably long. For practical purposes an appropriate compensation time could be chosen first, and then the corresponding compensation temperature could be obtained for optimizing the fixing efficiency. However, in the H–L procedure, the recording of the electronic grating and the proton–electron compensation both occur simultaneously at high temperature. In this case the key for optimization is to record the ionic grating such that it is as strong as possible. Because of the photovoltaic effect, which arises under light illumination, the grating strength oscillates during the recording phase. Hence we could select the temperature and the time such that the recording and compensation process ends when the modulation of the ionic grating, $n_{i1}(t)$, reaches the first local maximum. For this case we could first choose an appropriate recording and compensation temperature, and then the corresponding recording time is automatically obtained.

The authors acknowledge project support from National Science Council of the Republic of China contracts NSC87-2215-E009-011 and NSC88-2215-E009-008.

References

1. J. J. Amodei and D. L. Staebler, "Holographic pattern fixing in electrooptic crystals," Appl. Phys. Lett. **18,** 540–542 (1971).
2. D. L. Staebler, W. J. Burke, W. Philips, and J. J. Amodei, "Multiple storage and erasure of fixed holograms in Fe-doped $LiNbO_3$," Appl. Phys. Lett. **26,** 182–184 (1975).
3. R. Matull and R. A. Rupp, "Microphotometric investigation of fixed holograms," J. Phys. D **21,** 1556–1565 (1988).
4. P. Hertel, K. H. Ringhofer, and R. Sommerfeldt, "Theory of thermal hologram fixing and application to $LiNbO_3$:Cu," Phys. Status Solidi A **104,** 855–862 (1987).
5. V. V. Kulikov and S. I. Stepanov, "Mechanisms of holographic recording and thermal fixing in photorefractive $LiNbO_3$:Fe," Sov. Phys. Solid State **21,** 1849–1851 (1979).
6. G. Montemezzani and P. Guter, "Thermal hologram fixing in pure and doped $KNbO_3$ crystal," J. Opt. Soc. Am. B **7,** 2323–2328 (1990).
7. J. F. Heanue, M. C. Bashaw, A. J. Daiber, R. Snyder, and L. Hesselink, "Digital holographic storage system incorporating thermal fixing in lithium niobate," Opt. Lett. **21,** 1615–1617 (1996).
8. A. Mendez and L. Arizmendi, "Maximum diffraction efficiency of fixed holograms in lithium niobate," Opt. Mater. **10,** 55–59 (1998).
9. B. I. Sturman, M. Carrascosa, F. Agullo-Lopez, and J. Limeres, "Two kinetic regimes for high-temperature photorefractive phenomena in LiNbO3," J. Opt. Soc. Am. B **15,** 148–151 (1998).
10. U. Schlarb and K. Betzler, "Refractive indices of lithium niobate as function of temperature, wavelength, and composition: a generalized fit," Phys. Rev. B **48,** 15,613–15,620 (1993).
11. A. Mehta, E. K. Chang, and D. M. Smyth, "Ionic transport in LiNbO3," J. Mater. Res. **6,** 851–854 (1991).
12. S. Orlov, D. Psaltis, and R. R. Neurgaonkar, "Dynamic elec-

tronic compensation of fixed gratings in photorefractive materials," Appl. Phys. Letts. **63,** 2466–2468 (1993).
13. H. Vormann, G. Weber, S. Kapphan, and E. Kratzig, "Hydrogen as origin of thermal fixing in $LiNbO_3$:Fe," Solid State Commun. **40,** 543–545 (1981).
14. J. M. Cabrera, J. Olivarest, M. Carrascosa, J. Rams, R. Muller, and E. Dieguez, "Hydrogen in lithium niobate," Adv. Phys. **45,** 349–392 (1996).
15. B. I. Sturman, M. Carrascosa, F. Agullo-Lopez, and J. Limeres, "Theory of high-temperature photorefractive phenomena in $LiNbO_3$ crystals and applications to experiment," Phys. Rev. B **57,** 792–805 (1990).
16. M. Carrascosa and L. Arizmendi, "High-temperature photorefractive effects in $LiNbO_3$:Fe," J. Appl. Phys. **73,** 2709–2713 (1993).
17. A. Yariv, S. Orlov, G. Rakuljic, and V. Leyva, "Holographic fixing, read-out, and storage dynamics in photorefractive materials," Opt. Lett. **20,** 1334–1336 (1995).
18. M. Carrascosa and F. Agullo-Lopez, "Theoretical modeling of the thermal fixing and developing of holographic grating in $LiNbO_3$," J. Opt. Soc. Am. B **7,** 2317–2322 (1990).
19. J. D. Zook, D. Chen, and G. N. Otto, "Temperature dependence and model of the electro-optic effect in $LiNbO_3$," Appl. Phys. Lett. **11,** 159–161 (1967).
20. G. Montenmezzani, M. Zgonik, and P. Gunter, "Photorefractive charge compensation at elevated temperatures and application to $KNbO_3$," J. Opt. Soc. Am. B **10,** 171–185 (1993).
21. B. Liu, L. Liu, and L. Xu, "Characteristics of recording and thermal fixing in lithium niobate," Appl. Opt. **37,** 2170–2176 (1998).
22. N. V. Kukhtarev, V. B. Markov, S. G. Odulov, M. S. Soskin, and V. L. Vinetskii, "Holographic storage in electro-optics crystals. I. Steady state," Ferroelectrics **22,** 949–960 (1979).
23. C. Gu, J. Hong, H. Y. Li, D. Psaltis, and P. Yeh, "Dynamics of grating formation in photovoltaic media," J. Appl. Phys. **69,** 1167–1172 (1991).